PAPER

Silver(I) supramolecular complexes generated from isophorone-based ligands: crystal structures and enhanced nonlinear optical properties through metal complexation†

Zheng Zheng,[a] Zhi-Peng Yu,[a] Ming-Di Yang,[a] Feng Jin,*[a,b] Li-Na Ye,[a] Min Fang,[a] Hong-Ping Zhou,*[a] Jie-Ying Wu[a] and Yu-Peng Tian[a,c]

By self-assembly of (*E*)-2-(3-(4-(1*H*-imidazol-1-yl)styryl)-5,5-dimethylcyclohex-2-enylidene)malononitrile (**L¹**) and (*E*)-2-(3-(4-(1*H*-1,2,4-triazol-1-yl)styryl)-5,5-dimethylcyclohex-2-enylidene)malononitrile (**L²**) with silver(I) salts, eight new complexes, namely $AgL^1_2ClO_4$ (**1**), $AgL^1_2NO_3$ (**2**), $[AgL^1_2NO_3]\cdot C_6H_6$ (**3**), $[AgL^1_2OOCCF_3]\cdot C_6H_6$ (**4**), $[AgL^1_2PF_6]\cdot C_6H_6$ (**5**), $AgL^2_2NO_3$ (**6**), $[AgL^2OOCCF_3]_2$ (**7**) and $AgL^2_2PF_6$ (**8**), are presented along with an analysis of their structural features. The structures are built up through the combination of coordination bonds, $Ag\cdots\pi$, $Ag\cdots F$ (or O), hydrogen bonding, and $\pi\cdots\pi$ stacking interactions to generate new supramolecular architectures. We observed the formation of two-dimensional coordination polymers for complex **7**. Solvent benzene molecules and anions are dispersed in the supramolecular structure and play a vital role in building the supramolecular structures of the complexes. The nonlinear optical (NLO) properties of the complexes were investigated using the *Z*-scan technique and complexes **1**, **2**, **3**, **4** and **7** show obviously nonlinear absorption compared with ligands (**L¹** and **L²**).

Introduction

In recent years, the design and synthesis of metal–organic complexes based on strong coordinate bonds and multiple weak non-covalent forces have become one of the most active fields in coordination chemistry and crystal engineering due to their fascinating structural features and interesting properties.[1] Many supramolecular coordination complexes with specific topologies and excellent properties have been synthesized by assembly of metal salts and organic ligands.[2] Hence, in order to synthesize specific coordination complexes, many strategies have been studied and used by researchers.[3] However, at present it is still a challenge for chemists to predict and control the structures of such metal–organic

complexes, owing to the complicated influencing factors of the assembly reactions, such as the organic ligands, anions, the nature of transition metal ions and the experimental conditions like solvent, metal-to-ligand ratio and the reaction temperature.

The design and synthesis of new organic ligands is the key approach for construction of metal–organic complexes with desired structures and properties.[4] At present, it is still a challenge to synthesize new organic ligands in supramolecular architectures because of the synthetic difficulties involved. In designing coordination complexes, imidazolyl, triazolyl and cyano derivatives have been widely used as ligands due to their ability to coordinate to several metal centers in various modes.[5] Two new multidentate ligands based on isophorone, namely, (*E*)-2-(3-(4-(1*H*-imidazol-1-yl)styryl)-5,5-dimethylcyclohex-2-enylidene)malononitrile (**L¹**) and (*E*)-2-(3-(4-(1*H*-1,2,4-triazol-1-yl)styryl)-5,5-dimethylcyclohex-2-enylidene)malononitrile (**L²**)[6] have been used to construct new coordination complexes with specific structures and properties. On the other hand, Ag(I), as a soft Lewis acid, may adopt various coordination modes such as linear, trigonal planar, trigonal pyramidal and tetrahedral coordination geometries.[7] So, the combination of rigid organic spacers (**L¹** and **L²**) and Ag(I) metal ions would allow the formation of fascinating structural

[a]*College of Chemistry and Chemical Engineering, Anhui University, Key Laboratory of Functional Inorganic Materials Chemistry of Anhui Province, 230601 Hefei, P. R. China. E-mail: zhpzhp@263.net; Fax: +86-551-5107342; Tel: +86-551-5108151*
[b]*Department of Chemistry, Fuyang Normal College, Fuyang 236041, P. R. China*
[c]*State Key Laboratory of Coordination Chemistry, Nanjing University, Nanjing 210093, P. R. China*
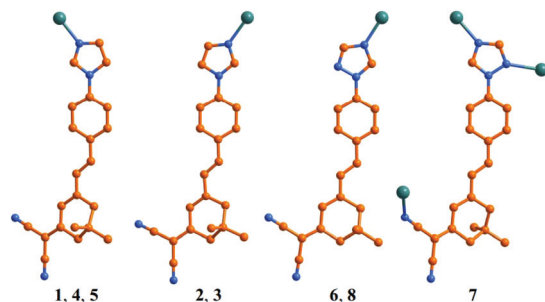
Scheme 1 The coordination modes of ligands L^1 and L^2 in complexes **1–8**.

diversities and interesting properties. Besides the ligand and metal centre, the anions, as charge-balance components, can adjust the topologies and properties of complexes through different coordinate bonds or non-covalent interactions.[8,9] Thus, when designing the coordination-driven architectures, the roles of the metal centre, anion, solvent and ligand all need to be considered. In this study, the syntheses and structures of eight novel Ag(I) complexes based on L^1 or L^2 and various Ag(I)X salts (X = ClO_4^-, NO_3^-, $OOCCF_3^-$ and PF_6^-) are described (Scheme 1). The third-order nonlinear optical (NLO) properties were measured by the Z-scan method. The results indicate that the two-photon absorption (TPA) coefficient β and TPA cross section σ of complexes **1**, **2**, **3**, **4** and **7** are larger than those of complexes **5**, **6**, **8** and free ligands (L^1 or L^2). The detailed structure–properties relationships are discussed.

Experimental section

General procedure

All commercially available chemicals and solvents are of reagent grade and were used as received without further purification. Elemental analyses were carried out on Perkin-Elmer 240 analyzer. IR spectra were recorded with a Nicolet FT-IR NEXUS 870 spectrometer (KBr discs) in the 4000–400 cm^{-1} region.

X-ray crystallography and structure solution

The X-ray diffraction measurements were performed on a Bruker SMART CCD area detector using graphite monochromated MoKα radiation (λ = 0.71069 Å) at 298(2) K. Intensity data were collected in the variable ω-scan mode. The structures were solved by direct methods and difference Fourier syntheses. The non-hydrogen atoms were refined anisotropically and hydrogen atoms were introduced geometrically. Calculations were performed with the SHELXTL-97 program package. Crystallographic data (excluding structure factors) for the structures reported in this paper have been deposited with the Cambridge Crystallographic Data Centre as supplementary publication no. CCDC: 917019, 917020, 917021, 917022, 917023, 917024, 917025, 917026. Details of the crystal

parameters, data collections and refinements for the complexes are summarized in Table 1, and selected bond distances and angles are listed in Table 2.

Synthesis of the complexes

AgL^1$_2$ClO$_4$ (1). L^1 (0.340 g, 1 mmol) in 25 mL of dichloromethane was added into a 50 mL colorimeter tube and carefully layered with a clear benzene solution (25 mL) of AgClO$_4$·H$_2$O (0.112 g, 0.5 mmol). Yellow, needle-like crystals suitable for single crystal X-ray diffraction were obtained by slow interlayer diffusion. Yield: 0.32 g (72%). Anal. Calc. for C$_{44}$H$_{40}$AgClN$_8$O$_4$: C, 59.50; H, 4.54; N, 12.62. Found: C, 59.32; H, 4.49; N, 12.67%. IR ν (cm^{-1}): 3133 (m), 2948 (m), 2926 (m), 2869 (w), 2218 (s, –C≡N), 1563 (s), 1519 (s), 1398 (w), 1332 (s), 1308 (m), 1188 (m), 1085 (s), 962 (m), 854 (m), 818 (m).

AgL^1$_2$NO$_3$ (2). L^1 (0.340 g, 1 mmol) in 25 mL of dichloromethane was added into a 50 mL colorimeter tube and carefully layered with a clear benzene solution (25 mL) of AgNO$_3$ (0.085 g, 0.5 mmol). Yellow, needle-like crystals suitable for single crystal X-ray diffraction were obtained by slow interlayer diffusion. Yield: 0.28 g (66%). Anal. Calc. for C$_{44}$H$_{40}$AgN$_9$O$_3$: C, 62.12; H, 4.74; N, 14.82. Found: C, 61.80; H, 4.69; N, 14.95%. IR ν (cm^{-1}): 3121 (m), 2951 (m), 2926 (m), 2868 (w), 2217 (s, –C≡N), 1565 (s), 1520 (s), 1384 (s), 1339 (s), 1305 (s), 1186 (m), 1130 (m), 1063 (s), 960 (s), 852 (m), 817 (m).

[AgL^1$_2$NO$_3$]·C$_6$H$_6$ (3). L^1 (0.340 g, 1 mmol) in 25 mL of dichloromethane was added into a 50 mL colorimeter tube and carefully layered with a clear methanol and benzene mixed solution (25 mL) of AgNO$_3$ (0.085 g, 0.5 mmol). Yellow, needle-like crystals suitable for single crystal X-ray diffraction were obtained by slow interlayer diffusion. Yield: 0.38 g (82%). Anal. Calc. for C$_{50}$H$_{46}$AgN$_9$O$_3$: C, 64.66; H, 4.99; N, 13.57. Found: C, 64.56; H, 5.03; N, 13.50%. IR ν (cm^{-1}): 3127 (m), 2955 (m), 2925 (m), 2868 (w), 2219 (s, –C≡N), 1562 (s), 1520 (s), 1384 (s), 1326 (s), 1278 (s), 1156 (m), 1051 (w), 972 (s), 851 (m), 813 (m).

Complexes **4–8** were prepared by a similar procedure. A clear acetonitrile and benzene mixed solution (25 mL) of the silver salt AgX (0.5 mmol, X = OOCCF$_3^-$ **4**, **7**, PF$_6^-$ **5**, NO$_3^-$ **6**, ClO$_4^-$ **7**,) was carefully layered onto a solution of L^1 or L^2 (0.341 g, 1 mmol) in dichloromethane (25 mL). Single crystals of **4–8** suitable for single crystal X-ray diffraction analyses were obtained by slow interlayer diffusion.

[AgL^1$_2$OOCCF$_3$]·C$_6$H$_6$ (4). Yield: 0.33 g (67%). Anal. Calc. for C$_{52}$H$_{46}$AgF$_3$N$_8$O$_2$: C, 63.74; H, 4.73; N, 11.44. Found: C, 63.58; H, 4.81; N, 11.38%. IR ν (cm^{-1}): 3125 (m), 2949 (m), 2926 (m), 2870 (w), 2217 (s, –C≡N), 1688 (s), 1564 (s), 1519 (s), 1398 (w), 1332 (m), 1308 (m), 1193 (m), 1129 (m), 1061 (s), 962 (s), 854 (m), 817 (m).

[AgL^1$_2$PF$_6$]·C$_6$H$_6$ (5). Yield: 0.38 g (75%). Anal. Calc. for C$_{50}$H$_{46}$AgF$_6$N$_8$P: C, 59.35; H, 4.58; N, 11.07. Found: C, 59.54; H, 4.39; N, 11.02%. IR ν (cm^{-1}): 3154 (m), 2949 (m), 2925 (m), 2870 (w), 2218 (s, –C≡N), 1564 (s), 1520 (s), 1398 (w), 1332 (m), 1308 (m), 1189 (m), 1131 (m), 1064 (m), 964 (m), 841 (s).

AgL^2$_2$NO$_3$ (6). Yield: 0.33 g (78%). Anal. Calc. for C$_{42}$H$_{38}$AgN$_{11}$O$_3$: C, 59.16; H, 4.49; N, 18.07. Found: C, 59.01; H,

Table 1 Crystallographic data for **1–8**

	1	**2**	**3**	**4**
Empirical formula	$C_{44}H_{40}AgClN_8O_4$	$C_{44}H_{40}AgN_9O_3$	$C_{50}H_{46}AgN_9O_3$	$C_{52}H_{46}AgF_3N_8O_2$
Formula weight	888.16	850.72	928.83	979.84
Crystal system	Triclinic	Monoclinic	Triclinic	Triclinic
Space group	$P\bar{1}$	$P2_1/c$	$P\bar{1}$	$P\bar{1}$
a [Å]	9.556(5)	7.727(5)	6.991(14)	9.667(5)
b [Å]	11.468(5)	32.015(5)	13.22(3)	11.899(5)
c [Å]	22.267(5)	8.917(5)	13.23(3)	21.743(5)
α [°]	93.896(5)	90	80.11(2)	93.227(5)
β [°]	98.182(5)	112.829(5)	81.34(2)	99.083(5)
γ [°]	100.288(5)	90	77.57(2)	100.103(5)
V [Å³]	2365.6(17)	2033.1(18)	1168(4)	2422.3(17)
Z	2	2	1	2
T [K]	298(2)	298(2)	293(2)	298(2)
D_{calcd} [g cm⁻³]	1.247	1.390	1.320	1.343
μ [mm⁻¹]	0.529	0.547	0.483	0.476
θ Range [°]	1.81–25.00	1.27–25.00	1.57–25.00	0.95–25.00
Total no. data	16 709	14 283	8274	17 293
No. unique data	8225	3572	4059	8460
No. params refined	572	306	303	599
R_1	0.0880	0.0524	0.0459	0.0686
wR_2	0.2129	0.1542	0.1199	0.2099
GOF	1.025	1.038	1.057	1.020

	5	**6**	**7**	**8**
Empirical formula	$C_{50}H_{40}AgF_6N_8P$	$C_{42}H_{38}AgN_{11}O_3$	$C_{46}H_{38}Ag_2F_6N_{10}O_4$	$C_{42}H_{38}AgF_6N_{10}P$
Formula weight	1005.74	852.70	1124.60	935.66
Crystal system	Triclinic	Monoclinic	Triclinic	Monoclinic
Space group	$P\bar{1}$	$C2/c$	$P\bar{1}$	$C2/c$
a [Å]	9.738(2)	26.621(5)	10.750(5)	26.768(5)
b [Å]	11.756(2)	7.851(5)	12.813(5)	7.990(5)
c [Å]	21.462(4)	18.755(5)	20.012(5)	19.600(5)
α [°]	94.268(3)	90	73.540(5)	90
β [°]	96.334(3)	92.618(5)	80.240(5)	96.028(5)
γ [°]	98.170(3)	90	65.257(5)	90
V [Å³]	2407.1(9)	3916(3)	2396.7(16)	4169(3)
Z	2	4	2	4
T [K]	298(2)	298(2)	298(2)	298(2)
D_{calcd} [g cm⁻³]	1.388	1.446	1.558	1.491
μ [mm⁻¹]	0.518	0.570	0.894	0.593
θ Range [°]	1.76–25.00	1.53–25.00	1.06–25.00	1.53–25.00
Total no. data	17 215	13 435	16 562	14 264
No. unique data	8383	3445	8307	3669
No. params refined	599	261	617	274
R_1	0.0688	0.0389	0.0614	0.0351
wR_2	0.1746	0.1121	0.1649	0.0965
GOF	1.049	1.002	1.063	1.025

4.56; N, 17.95%. IR ν (cm⁻¹): 3128 (m), 2956 (m), 2925 (m), 2869 (w), 2218 (s, –C≡N), 1561 (s), 1514 (s), 1384 (s), 1319 (s), 1279 (m), 1158 (m), 972 (s), 850 (m).

[**AgL²OOCCF₃**]₂ (**7**). Yield: 0.20 g (71%). Anal. Calc. for $C_{46}H_{38}Ag_2F_6N_{10}O_4$: C, 49.13; H, 3.41; N, 12.45. Found: C, 48.97; H, 3.52; N, 12.21%. IR ν (cm⁻¹): 3084 (w), 2950 (m), 2919 (m), 2870 (w), 2218 (s, –C≡N), 1675 (s), 1563 (s), 1522 (s), 1416 (m), 1330 (m), 1278 (m), 1205 (s), 1139 (s), 973 (s), 857 (m).

AgL²₂PF₆ (**8**). Yield: 0.37 g (80%). Anal. Calc. for $C_{42}H_{38}AgF_6N_{10}P$: C, 53.91; H, 4.09; N, 14.97. Found: C, 53.72; H, 4.24; N, 14.73%. IR ν (cm⁻¹): 3162 (m), 2950 (m), 2927 (m), 2869 (w), 2217 (s, –C≡N), 1564 (s), 1523 (s), 1399 (m), 1325 (s), 1289 (m), 1230 (w), 1154 (m), 976 (s), 845 (m).

Results and discussion

Synthesis and structural analysis

Compounds **1–8** were obtained as supramolecular complexes by combination of **L¹** or **L²** with different inorganic Ag(I) salts. Well-shaped X-ray quality crystals of **1–8** were obtained by direct metal–ligand assembly in different solvents. As a result, complexes **1** and **2** were isolated from CH_2Cl_2–C_6H_6, and **3** was isolated from CH_2Cl_2–CH_3OH–C_6H_6, whereas **4–8** were isolated from CH_2Cl_2–CH_3CN–C_6H_6. All eight complexes were fully characterized by IR spectra and elemental analysis. Compared to ligand **L¹**, **L²** is endowed with more structural potential. The two coordinating sites on the triazole ring could serve as an additional coordinating donors compared with **L¹**, which is

Table 2 Selected bond lengths (Å) and angles (°) for **1–8**

$[C_{22}H_{20}N_4]_2 \cdot AgClO_4$ (**1**)					
Ag(1)–N(4)	2.083(6)	Ag(1)–N(5)	2.103(6)	N(4)–Ag(1)–N(5)	178.9(3)
$[C_{22}H_{20}N_4]_2 \cdot AgNO_3$ (**2**)					
Ag(1)–N(4)	2.117(3)	Ag(1)–N(4)A	2.117(3)	N(4)A–Ag(1)–N(4)	180.000(1)
$[C_{22}H_{20}N_4]_2 \cdot AgNO_3 \cdot C_6H_6$ (**3**)					
Ag(1)–N(1)	2.186(5)	Ag(1)–N(1)A	2.186(5)	N(1)A–Ag(1)–N(1)	180.00(14)
$[C_{22}H_{20}N_4]_2 \cdot AgOOCCF_3 \cdot C_6H_6$ (**4**)					
Ag(1)–N(4)	2.104(4)	Ag(1)–N(5)	2.110(4)	Ag(1)–O(1)	2.552(6)
N(4)–Ag(1)–N(5)	170.24(16)	N(4)–Ag(1)–O(1)	91.59(18)	N(5)–Ag(1)–O(1)	97.74(18)
$[C_{22}H_{20}N_4]_2 \cdot AgPF_6 \cdot C_6H_6$ (**5**)					
Ag(1)–N(4)	2.072(5)	Ag(1)–N(5)	2.090(5)	N(4)–Ag(1)–N(5)	175.4(2)
$[C_{21}H_{19}N_5]_2 \cdot AgNO_3$ (**6**)					
Ag(1)–N(1)	2.120(2)	Ag(1)–N(1)A	2.120(2)	N(1)–Ag(1)–N(1)A	166.12(13)
$[C_{21}H_{19}N_5]_2 \cdot [AgOOCCF_3]_2$ (**7**)					
Ag(1)–N(6)	2.144(4)	Ag(1)–N(5)	2.171(4)	Ag(1)–O(1)	2.501(4)
Ag(2)–O(2)	2.304(5)	Ag(2)–O(4)	2.309(5)	Ag(2)–N(2)	2.351(7)
Ag(2)–N(4)	2.403(4)	N(6)–Ag(1)–N(5)	167.74(14)	N(6)–Ag(1)–O(1)	106.51(15)
N(5)–Ag(1)–O(1)	85.75(15)	O(2)–Ag(2)–O(4)	121.65(19)	O(2)–Ag(2)–N(2)	111.9(3)
O(4)–Ag(2)–N(2)	111.2(3)	O(2)–Ag(2)–N(4)	114.45(18)	O(4)–Ag(2)–N(4)	83.21(15)
N(2)–Ag(2)–N(4)	111.2(2)				
$[C_{21}H_{19}N_5]_2 \cdot AgPF_6$ (**8**)					
Ag(1)–N(5)	2.114(2)	Ag(1)–N(5)A	2.114(2)	N(5)–Ag(1)–N(5)A	175.44(13)

one of the most important factors in control of the polymeric motifs. Furthermore, in complex **7**, it is worthwhile to point out that the cyano of ligand has the ability to coordinate Ag(ɪ).[5c] In these Ag(ɪ) compounds, different coordination modes of triazole-containing ligand L^2 were observed, which result in the polymeric structure of complex **7** not achievable by other rigid linear organic spacers. In this paper, the crystal structures were divided into two groups with different ligands: L^1 (**1–5**) and L^2 (**6–8**), respectively, to discuss the structures of the silver complexes.

Crystal structure of complexes 1–5 based on L^1

Single crystal X-ray diffraction analyses provide direct evidence for the structure of the complexes, and the results showed that **1**, **3**, **4**, **5** crystallize in the same triclinic space group $P\bar{1}$ (Table 1), and have similar supramolecular structures. As shown in Fig. 1a, 3a–5a, L^1 adopts the *trans*-conformation to bind Ag(ɪ) ions with two imidazolyl nitrogen atoms from two different molecules in **1**, **3**, **4** and **5**. The bond angle of N–Ag–N is 178.9(3)° for **1**, 180.00(14)° for **3**, 170.24(16)° for **4** and
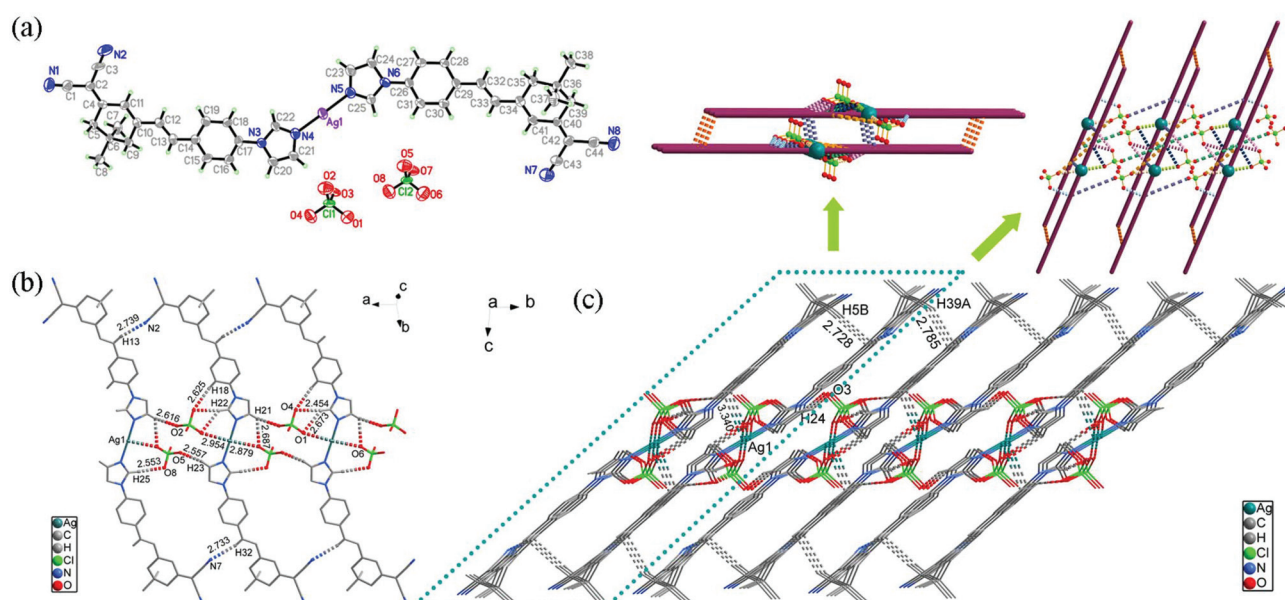

Fig. 1 (a) ORTEP drawing of **1** with the ellipsoids drawn at the 30% probability level. (b) The 1D chain structure of complex **1** formed by multiple C−H⋯O hydrogen bonding and Ag⋯O interactions. (c) The 2D layer structure of complex **1** formed by multiple C−H⋯O hydrogen bonding, Ag⋯π interactions and C−H⋯π interactions. Dotted lines represent the weak interactions. Hydrogen atoms not participating in hydrogen bonding are omitted for clarity.
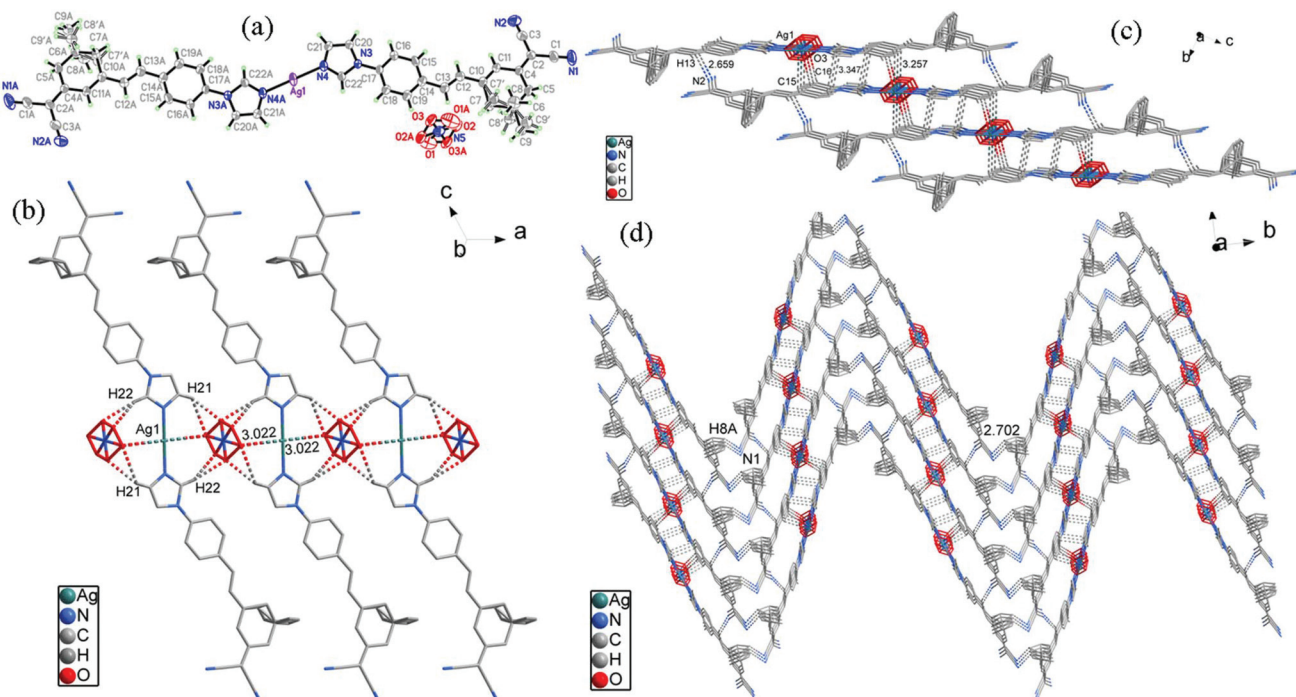
Fig. 2 (a) ORTEP drawing of **2** with the ellipsoids drawn at the 30% probability level. (b) The 1D chain structure of complex **2** formed by multiple C–H⋯O hydrogen bonding and Ag⋯O interactions. (c) The 2D layer structure of complex **2** formed by C–H⋯N hydrogen bonding, Ag⋯π interactions, C–H⋯O hydrogen bonding and π⋯π interactions. (d) The 3D supramolecular structure of complex **2** formed by multiple C–H⋯N hydrogen bonding interactions. Dotted lines represent the weak interactions. Hydrogen atoms not participating in hydrogen bonding are omitted for clarity.

175.4(2)° for **5**, indicating a linear coordination geometry.[10] The deviation of the value of the N–Ag–N angle for **1**, **4** and **5** is probably due to the internal steric hindrance between the anions and the two coordinated ligand molecules. The Ag–N bond lengths of **1**, **3**, **4** and **5** fall within the normal range as seen in Table 2.[11] Furthermore, the Ag(I) cation in each complex is charge balanced by free anions while CF_3COO^- anions have strong coordination ability and they coordinate with Ag(I) ions in the $AgL^1_2OOCCF_3 \cdot C_6H_6$ (**4**) unit.[12] The disorder appears in the O atoms of the free nitrate anion in complex **3**.

Fig. 1b and 3b indicate that the uncoordinated perchlorate and nitrate anions play a significant role in forming a 1D chain structure through Ag⋯O interactions with distances in the range of 2.736–2.954 Å and various C–H⋯O hydrogen bonds with distances in the range of 2.186–2.954 Å. Additionally, we can find that it is the weak force of C–H⋯N hydrogen bond ($d = 2.739$ Å) that constructs the 1D chain structure of **1**. However, different from **1** and **3**, the benzene molecules play a critical role in determining the 1D chain structure in the crystal packing of complexes **4** and **5** (Fig. 4b and 5b). Furthermore, the chains of **1**, **3** and **4** are further connected via intermolecular interactions to generate a layer structure (Fig. 1c, 3c and 4c). While in the crystal structure of complex **5** (Fig. 5c), multiple C–H⋯F hydrogen bonding interactions, including C28–H28⋯F2 ($d = 2.516$ Å), C20–H20⋯F3 ($d = 2.329$ Å) and C24–H24⋯F6 ($d = 2.365$ Å) based on the uncoordinated PF_6^- counterions are formed. The PF_6^- anions link the chains

together through multiple C–H⋯F hydrogen bonding interactions to generate a two-dimensional supramolecular structure.

Complex **2** was prepared from the same ligand (L^1) and metal salt (NO_3^-) as complex **3**. Different from **3**, the crystals of complex **2** were obtained from dichloromethane–benzene mixed solution. Compared to **3**, complex **2** crystallizes in the monoclinic form with space group $P2_1/c$ rather than in the triclinic space group $P\bar{1}$ as shown in Table 1. The molecular structure of complex **2** is illustrated in Fig. 2a. The ligand L^1 in **2** adopts the same coordination mode as complexes **1**, **3** and **5**. Complex **2** has the same linear coordination geometry as complexes **1**, **3** and **5**. The disorder appears in the O atoms of the free nitrate anion and C7, C8, C9 of the ligands. The adjacent mononuclear complex molecules are linked together along the *a*-axis through multiple C–H⋯O hydrogen bonds (O⋯H distances in the range of 2.278–2.680 Å) and Ag⋯O interactions ($d = 3.022$ Å) based on NO_3^- to form an infinite chain, as illustrated in Fig. 2b. The neighboring chains are further linked by intermolecular interactions, giving rise to an extended layer structure along the *c* plane, as shown in Fig. 2c. Seen along the *b*-axis in Fig. 2d, significantly different from complex **3**, the nitrogen atoms of –C≡N are not directly involved in coordination, but the lone pair electrons from the N atom still have a strong *pro-E* competence, which generates a 3D zigzag supramolecular structure through C8A–H8A⋯N1 hydrogen bonds ($d = 2.702$ Å).

The assembled reactions of L^1 with $AgNO_3$ by varying the solvent from CH_2Cl_2–C_6H_6 to CH_2Cl_2–CH_3OH–C_6H_6 afford
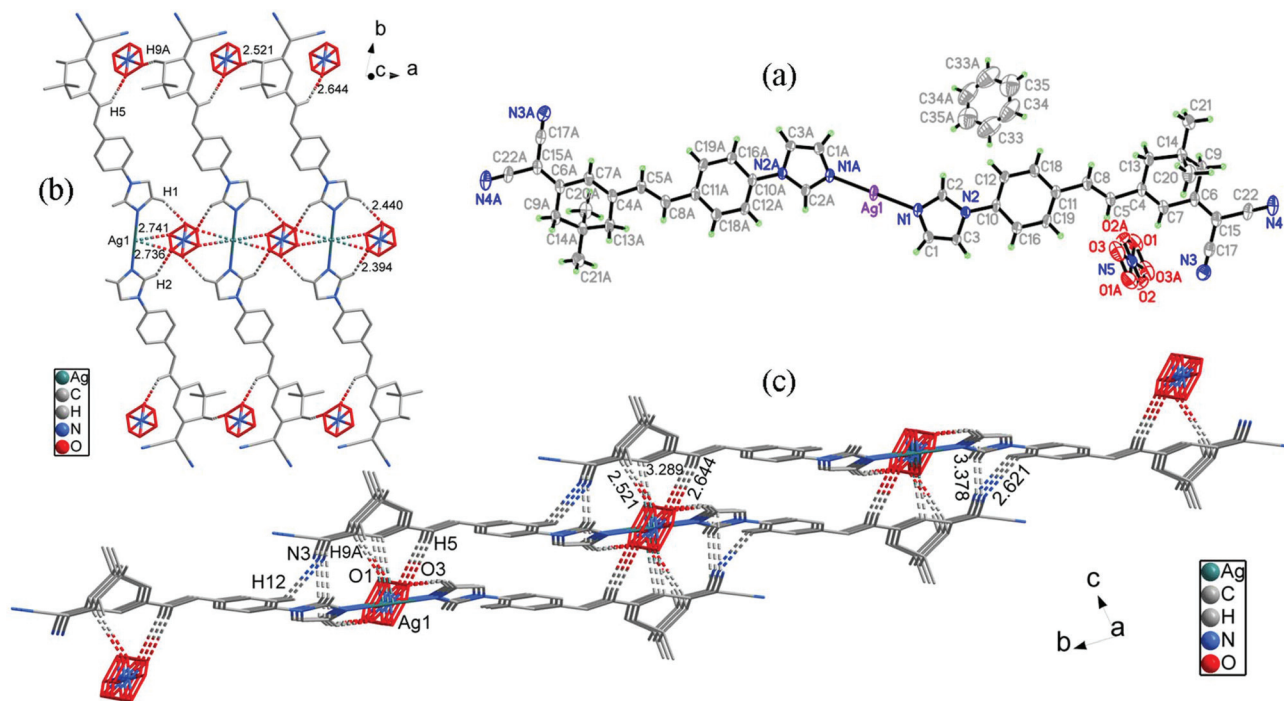
Fig. 3 (a) ORTEP drawing of **3** with the ellipsoids drawn at the 30% probability level. (b) The 1D chain structure of complex **3** formed by multiple C−H···O hydrogen bonding and Ag···O interactions. (c) The 2D layer structure of complex **3** formed by multiple C−H···O hydrogen bonding, C−H···N hydrogen bonding, Ag···π interactions and π···π interactions. Dotted lines represent the weak interactions. Hydrogen atoms not participating in hydrogen bonding are omitted for clarity.
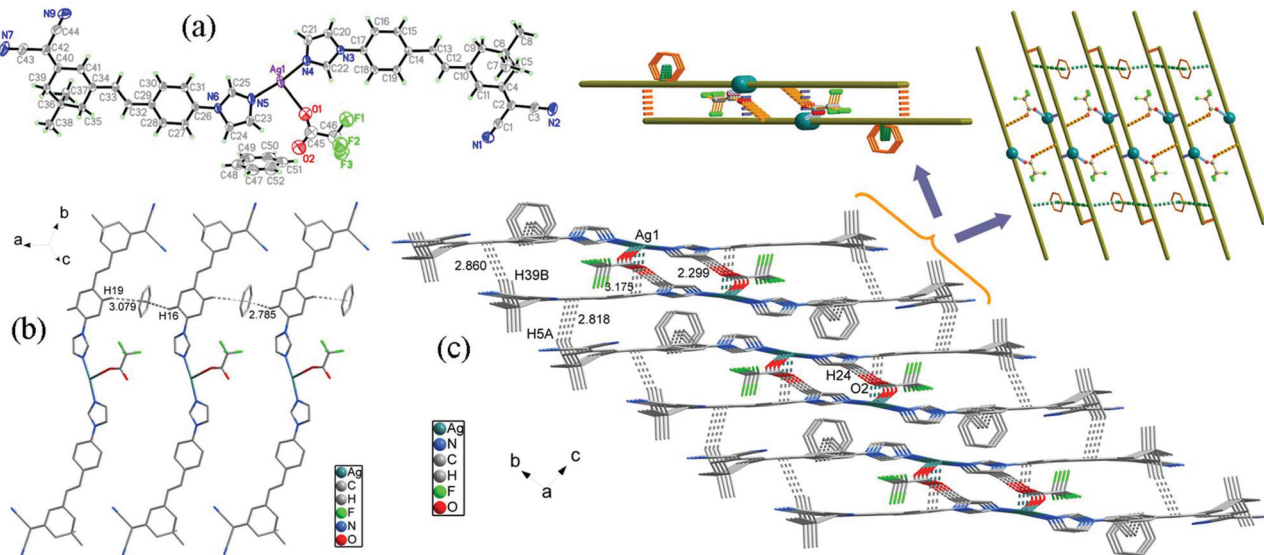
Fig. 4 (a) ORTEP drawing of **4** with the ellipsoids drawn at the 30% probability level. (b) The 1D chain structure of complex **4** formed by C−H···π interactions. (c) The 2D layer structure of complex **4** formed by C−H···O hydrogen bonding, Ag···π interactions and C−H···π interactions. Dotted lines represent the weak interactions. Hydrogen atoms not participating in hydrogen bonding are omitted for clarity.

complexes **2** and **3**, respectively. Taking complexes **2** and **3** into account, the main difference is the existence of solvent benzene molecules in complex **3** while there are no solvent molecules in complex **2**, which results in an extremely different supramolecular structure. In complex **2**, the final 3D

zigzag supramolecular structure along the *b*-axis is formed through C8A−H8A···N1 hydrogen bonds. The result shows that the steric hindrance of solvent benzene molecules in **3** have a direct influence on the formation of the 3D supramolecular structure.
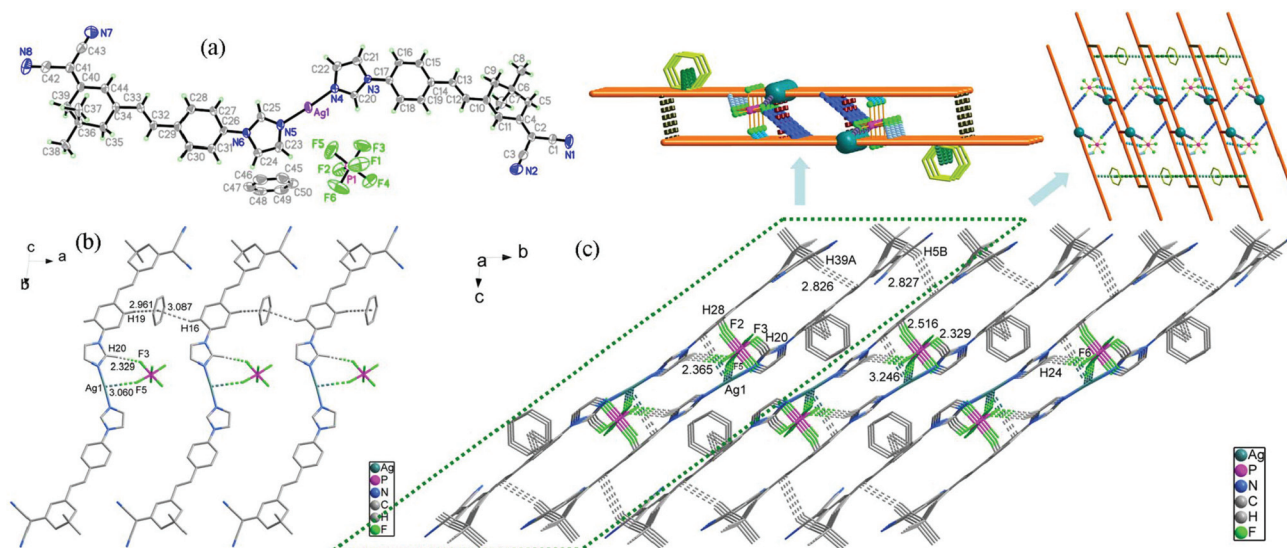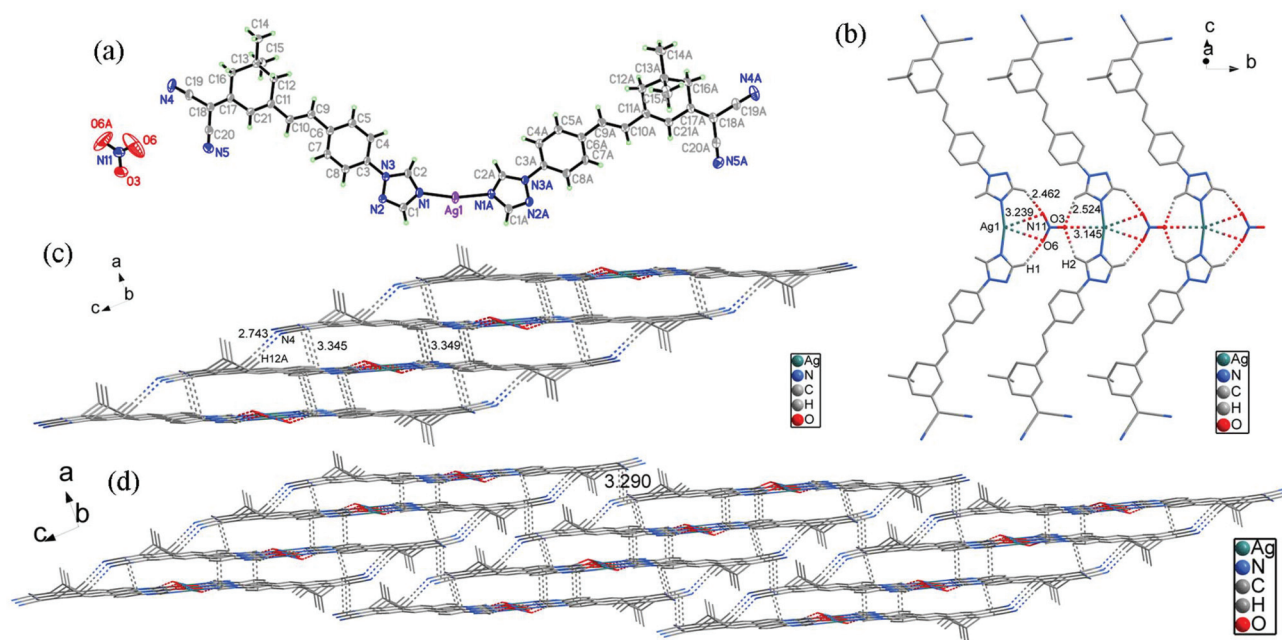
Fig. 5 (a) ORTEP drawing of **5** with the ellipsoids drawn at the 30% probability level. (b) The 1D chain structure of complex **5** formed by C−H⋯π interactions. (c) The 2D layer structure of complex **5** formed by multiple C−H⋯F hydrogen bonding, Ag⋯F interactions, Ag⋯π interactions and C−H⋯π interactions. Dotted lines represent the weak interactions. Hydrogen atoms not participating in hydrogen bonding are omitted for clarity.

Fig. 6 (a) ORTEP drawing of **6** with the ellipsoids drawn at the 30% probability level. (b) The 1D chain structure of complex **6** formed by multiple C−H⋯O hydrogen bonding and Ag⋯O interactions. (c) The 2D layer structure of complex **6** formed by C−H⋯N hydrogen bonding and π⋯π interactions. (d) The 3D supramolecular structure of complex **6** formed by π⋯π interactions. Dotted lines represent the weak interactions. Hydrogen atoms not participating in hydrogen bonding are omitted for clarity.

Crystal structure of complexes 6–8 based on L²

Complexes **6** and **8** crystallize in the same monoclinic $C2/c$ space group (Table 1). Fig. 6a and 8a show the coordination environments of the Ag(ɪ) ions with the atom numbering scheme. The ligand **L²**, quite different from **L¹** in complexes **1–5** and **7**, adopts the *cis*-conformation to bind Ag(ɪ) ions with

triazolyl moieties located on the same side of ligand in **6** and **8** as shown in Fig. 6a and 8a. The N1–Ag1–N1A and N5–Ag1–N5A angles deviate from 180.00° probably due to the influence of the weak C−H⋯O or C−H⋯F interactions. The Ag–N bond lengths (Table 2) are comparable to those in the reported Ag(ɪ) complexes.[11] Similar to **1–3**, the free anions play a significant role in forming the 1D chain structure along the *b*-axis
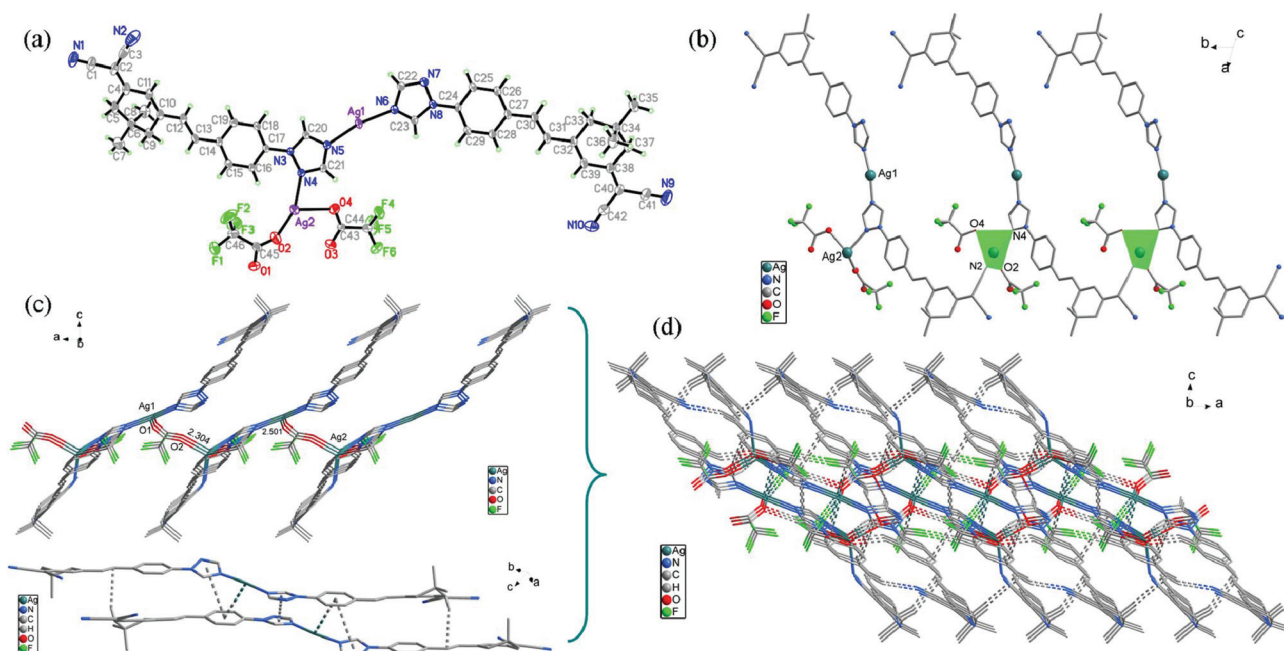
Fig. 7 (a) ORTEP drawing of 7 with the ellipsoids drawn at the 30% probability level. (b) The 1D chain structure of complex 7. (c) The 2D layer structure of complex 7 and (d) further formed by C–H···π interactions, Ag···π interactions and π···π interactions. Dotted lines represent the weak interactions. Hydrogen atoms not participating in hydrogen bonding are omitted for clarity.

through Ag···O interactions and various C–H···O hydrogen bonds based on NO_3^- anions for **6**, or through Ag···F interactions and various C–H···F hydrogen bonds based on PF_6^- anions for **8**. The neighboring chains are further linked by C12A–H12A···N4 (2.743 Å) and π–π stacking interactions (3.345 Å and 3.349 Å) for **6**, or by C15–H15···F1 (2.644 Å), C9B–H9B···F1 (2.464 Å) and π–π stacking interactions (3.321 Å) for **8**, giving rise to an extended layer staircase structure along the *c* plane, as shown in Fig. 6c and 8c, respectively. As shown in Fig. 6d and 8d, the uncoordinated –C≡N moieties of the ligand **L**^{2} play an important role in generating the 3D supramolecular structure along the *ac* plane through π···π interactions with the distance of 3.290 Å for **6** and 3.301 Å for **8**.

Single-crystal analysis indicates that complex **7** with two silver(ɪ) ions in the asymmetric unit crystallizes in the triclinic system, space group $P\bar{1}$. As shown in Fig. 7a, **L**^{2} adopts the *trans*-conformation to bind Ag1 ions with two triazolyl nitrogen atoms from two different molecules located on different sides of the ligand. The N6–Ag1–N5 angle is not 180.00° but 167.74(14)°, which should be due to the influence of the Ag1–O1 interactions. Notably, the two crystallographically independent Ag(ɪ) centers display different trigonal and tetrahedral coordination geometries, respectively (see Fig. 7c). Similar to **4**, the Ag1 center is also coordinated by one oxygen atom from CF_3COO^- due to their strong coordination ability, with the distance of 2.501 Å to form a trigonal planar geometry.[12] However, the Ag2 center is surrounded by two oxygen atoms from two F_3CCOO^- anions, one triazolyl nitrogen atom from one ligand and one –C≡N nitrogen atom from the other ligand to form a distorted tetrahedral geometry.[13] It is

noteworthy that the Ag2 ions bridge two neighboring Ag1L^2 units to generate a 1D coordination polymer with the Ag1···Ag2 distance of 6.433 Å (Fig. 7b). The chains are further connected *via* F_3CCOO^- to generate a layer structure of polymer **7** (Fig. 7c). The bond angles around the silver atom are in the range of 83.21(15)–167.74(14)°. Additionally, C37B–H37B···π, Ag···π and π···π interactions with distances of 2.895, 3.735 and 3.878 Å, respectively, provide further stability to the layer structure (Fig. 7d). The results indicate that the similar supramolecular structures of **6** and **8** are different from that of **7**, which is probably ascribed to the different coordination modes of the ligands **L**^{2} in **6**, **8** and **7** (Scheme 1).

Structural comparison and effect of ligands and anions on the structures

The diverse coordination modes of the organic ligands have been proven to have a great influence on the structure of complexes.[14] The coordination modes of the **L**^{1} and **L**^{2} ligands are shown in Scheme 1. The complexes containing **L**^{1} with different anions have an almost identical coordination sphere around the silver cation (except in **4**) and the arrangement of their building blocks is similar. Complexes **6** and **8** with **L**^{2} also have an almost identical coordination sphere around the silver cation and supramolecular structure, which is different from **1**–**5**. The **L**^{1} ligands in complexes **1**–**5** adopt the *trans*-conformation to bind Ag(ɪ) ions while they adopt the *cis*-conformation to bind Ag(ɪ) ions in complexes **6** and **8**. Obviously, the **L**^{1} and **L**^{2} ligands show distinct binding features upon metal complexation due to the imidazolyl group in **L**^{1} being replaced by the triazolyl in **L**^{2}. The structures of **1**–**6** and **8** show that
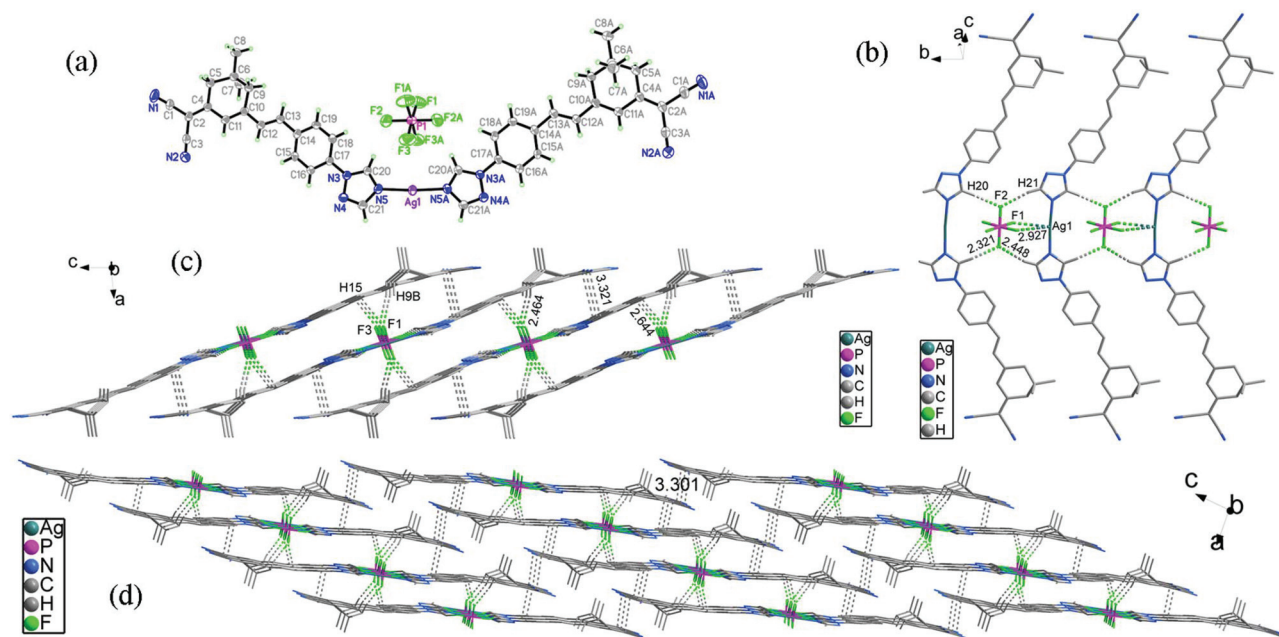
Fig. 8 (a) ORTEP drawing of **8** with the ellipsoids drawn at the 30% probability level. (b) The 1D chain structure of complex **8** formed by multiple C−H⋯F hydrogen bonding and Ag⋯F interactions. (c) The 2D layer structure of complex **8** formed by multiple C−H⋯F hydrogen bonding and π⋯π interactions. (d) The 3D supramolecular structure of complex **8** formed by π⋯π interactions. Dotted lines represent the weak interactions. Hydrogen atoms not participating in hydrogen bonding are omitted for clarity.

they are all mononuclear complexes and only one nitrogen atom of the imidazolyl group in **L¹** or the triazolyl group in **L²** is bound to the Ag(ɪ) atom. In the structures of **1–8**, it was found that there is one coordination F_3CCOO^- anion in **4** and **7**, while no coordinated anions were detected in **1**, **2**, **3**, **5**, **6** and **8**. For complex **7**, interestingly, two nitrogen atoms of the triazolyl group and one nitrogen atom of cyano group all co-ordinate with the Ag(ɪ) atoms in a special mode, to generate the 2D coordination polymer. The two Ag(ɪ) atoms in complex **7** adopt three-coordination and four-coordination respectively due to F_3CCOO^- chelating with two silver atoms. The results confirm that there are plentiful different coordination modes for the **L²** ligand in their silver metal complexes **6–8** and, furthermore, the F_3CCOO^- anion is easy to chelate with silver atoms compared with other anions. Additionally, the above new silver(ɪ) coordination complexes are built up through the combination of silver coordination, Ag⋯π, Ag⋯F (or O), hydrogen bonding, and π⋯π stacking interactions to generate new supramolecular architectures.[15]

Solvent benzene molecules are dispersed in the supramolecular structure and play a vital role in building the supramolecular structures by forming different C−H⋯π interactions in complexes **4** and **5**, while no weak interaction involving them was observed in the solid state of **3**. Different from **L¹**, the assembled systems of **L²** and Ag(ɪ) are also not sensitive to solvent media. It is worth pointing out that the ClO_4^-, NO_3^-, and PF_6^- anions are near to the Ag(ɪ) centre in their complexes and are weakly coordinated to the Ag(ɪ). It has been further demonstrated that anions also play an important role in

preparing coordination complexes, which can be divided into two key effects depending on the final supramolecular structure. The anions influence the coordination environment of the metal cations by coordination with them and which in turn dictates the construction of the supramolecular structure.

We are of the opinion that this study further leads to the systematic investigation of the supramolecular structure of silver coordination complexes based on weak interactions adjusted by the selection of different ligands, various anions and solvent molecules. This study demonstrates that the tri-azole-containing rigid organic ligand (*E*)-2-(3-(4-(1*H*-1,2,4-triazol-1-yl)styryl)-5,5-dimethylcyclohex-2-enylidene)malononi-trile (**L²**) is capable of coordinating metal centers with both N_{cyano} and $N_{triazole}$ donors, and generating novel coordination polymers.

Third-order nonlinear optical properties

The third-order NLO properties were measured at a concentration of 1.0×10^{-3} mol L⁻¹ in DMSO solution using the *Z*-scan technique. For the experiments, the pulse length was 140 fs and the repetition rate was kept at 10 Hz. Because **L²**, **L²**, **5**, **6** and **8** have no nonlinear absorption in DMSO, only the third-order optical nonlinearities of complexes **1**, **2**, **3**, **4** and **7** are presented. The excitation wavelengths of complexes **1**, **2**, **3**, **4** and **7** are 700, 750, 740, 720 and 740 nm, respectively.

The open aperture *Z*-scan curves are shown in Fig. 9(a) and Fig. S1 (ESI†). The filled squares represent the experimental data and the solid line is the theoretical data fitted by using
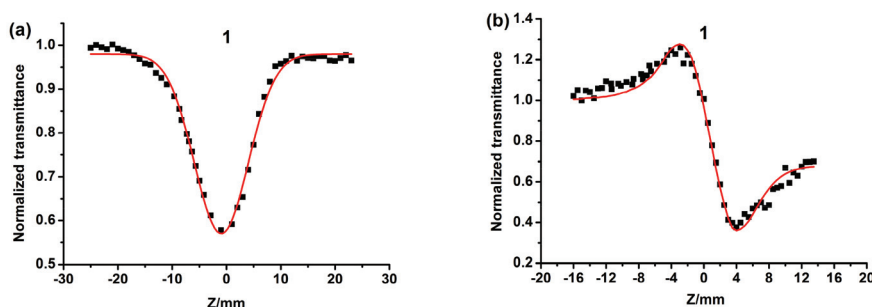
Fig. 9 (a) The open aperture and (b) close aperture Z-scan data of complex **1**. The filled squares represent the experimental data and the solid curve is the theoretical data.

the following equations:[16,17]

$$T(z, s = 1) = \sum_{m=0}^{\infty} \frac{[-q_0(z)]^m}{(m+1)^{3/2}} \text{ for } |q_0| < 1$$

$$q_0(z) = \frac{\beta I_0 L_{\text{eff}}}{1 + x^2}$$

where $x = z/z_0$, z is the distance of the sample and beam focus, $z_0 = \pi\omega_0^2/\lambda$ is the diffraction length of the beam with ω_0 the spot size at focus, λ is the wavelength of the beam, β is the TPA coefficient, I_0 is the input intensity at the focus ($z = 0$) calculated by the input energy divided by $\pi\omega_0^2$, $L_{\text{eff}} = (1 - e^{-\alpha L})/\alpha$ is the effective length with α the linear absorption coefficient and L the sample length. Furthermore, the molecular TPA cross-section (σ) could be determined by using the following relationship:[17]

$$\sigma = h\gamma\beta/N_A d \times 10^{-3}$$

here h is the Planck's constant, γ is the frequency of input intensity, N_A is the Avogadro constant, and d is the concentration of the sample. Based on the above equations, the values of β and σ of the complexes are given in Table 3. Obviously, the TPA coefficient β and TPA cross section σ of complexes **1**, **2**, **3**, **4** and **7** are larger than those of free ligands ($\mathbf{L^1}$, $\mathbf{L^2}$).

The nonlinear refraction indexes of complexes **1**, **2**, **3**, **4** and **7** were determined by the close aperture Z-scan technique. The resulting data and fitted curve are shown in Fig. 9(b) and Fig. S1 (ESI†). According to the figures, the reported complexes **1**, **2**, **3**, **4** and **7** exhibit a self-defocusing effect ($\Delta n < 0$) with a peak-to-valley configuration. The effective third-order NLO susceptibility $\chi^{(3)}$ of the sample can be calculated by the following

equations:[18]

$$R_e\chi^{(3)} = 10^{-4}n_0^2\varepsilon_0 c^2 \gamma/\pi$$

$$I_m\chi^{(3)} = 10^{-2}n_0^2\varepsilon_0 c^2 \beta\lambda/4\pi^2$$

$$\chi^{(3)} = \sqrt{(R_e\chi^{(3)})^2 + (I_m\chi^{(3)})^2}$$

where ε_0 is the vacuum permittivity, c is the light velocity in a vacuum and n_0 is the linear refractive index of DMSO. In this case, the third-order nonlinear refractive index γ can be derived from the equations:[19]

$$\Delta T_{\text{pv}} = 0.406(1 - S)^{0.25}|\Delta\varphi|, \quad \Delta\varphi = KL_{\text{eff}}\gamma I_0$$

In the equations, ΔT_{pv} is the difference between the peak and the valley of the normalized transmission, S is the fraction of the transmitted beam through the aperture, and $\Delta\varphi$ is the on-axis phase shift, where $\Delta T_{\text{pv}} = 0.92$ (**1**), 0.33 (**2**), 0.62 (**3**), 0.45 (**4**) and 0.40 (**7**), $S = 0.210$, $K = 2\pi/\lambda$. The obtained γ and $\chi^{(3)}$ are listed in Table 3.

Free ligands $\mathbf{L^1}$ and $\mathbf{L^2}$ do not show any nonlinear absorption behavior at ~700 nm. In contrast, significant nonlinear absorption performance is observed for each of the complexes **1**, **2**, **3**, **4** and **7** at the excitation wavelength which may be caused by cooperative intermolecular interactions in the complexes.[20] The isophorone ligands ($\mathbf{L^1}$, $\mathbf{L^2}$) belong to the D–π–A analogue since the terminal imidazole or triazole part possesses very weak electron-donating character. Complexation with Ag(I) enhances the electron-acceptor character of the imidazole or triazole moiety, converting $\mathbf{L^1}$ or $\mathbf{L^2}$ to a more strongly polarized A–π–D unit (Fig. 10) that makes the complexes **1**, **2**, **3**, **4** and **7** potential candidates for third-order nonlinear responses.

Table 3 Third-order NLO data for complexes **1**, **2**, **3**, **4** and **7**

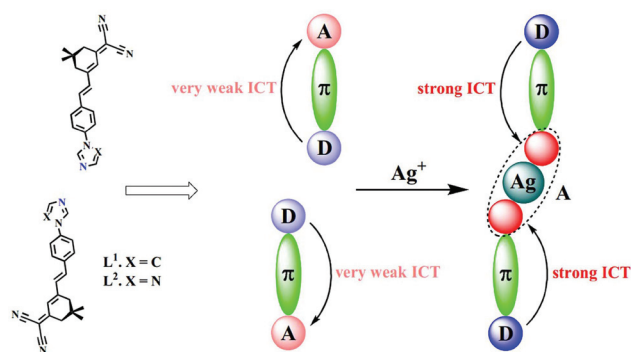| Complex	1	2	3	4	7
β (cm GW^{-1})	1.88	0.12	0.14	0.08	0.44
σ (cm^4 s photon^{-1} molecule^{-1})	8.86×10^{-46}	5.28×10^{-47}	6.24×10^{-47}	3.80×10^{-47}	1.96×10^{-46}
γ (m^2 W^{-1})	1.17×10^{-17}	5.12×10^{-18}	9.27×10^{-18}	6.22×10^{-18}	5.99×10^{-18}
$\chi^{(3)}$ (esu)	5.86×10^{-15}	4.90×10^{-16}	6.90×10^{-16}	4.35×10^{-16}	1.48×10^{-15}

Fig. 10 Plan for metal-mediated third-order nonlinear responses in D−π-A ligands.
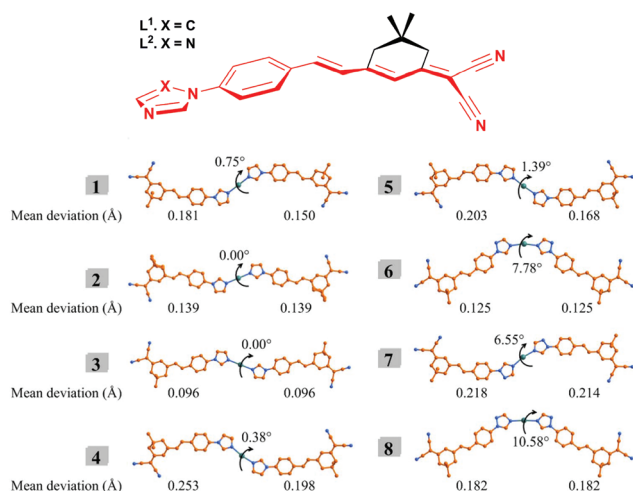

Fig. 11 The scheme of ligands and complexes, the 21 atoms forming the mean plane are drawn in red. The anions are omitted for clarity.

As shown in Fig. 11, the conjugated system of ligand (L^1 or L^2) in the complex is almost planar with 21 atoms forming a mean plane. The puckering amplitude to the mean plane for the 21 atoms Δ does not exceed 0.253 Å. The dihedral angles measured between the two mean planes in a complex unit are 0.75° (**1**), 0.00° (**2**), 0.00° (**3**), 0.38° (**4**), 1.39° (**5**), 7.78° (**6**), 6.55° (**7**) and 10.58° (**8**), respectively. Compared with complexes **1**, **2**, **3**, **4** and **7**, complexes **5**, **6** and **8** do not show any nonlinear absorption behavior, which is probably ascribed to the larger dihedral angle between the two mean planes, and the distorted conformations do not permit effective conjugation.[21] The enhanced nonlinear absorption is also observed for the complex **7** although it has a larger dihedral angle between the two mean planes, which is probably due to the formation of two-dimensional coordination polymers increasing the conjugation length of complex **7**. The results indicate that the effective intramolecular charge transfer and increased conjugation length in complexes **1**, **2**, **3**, **4** and **7** may be responsible for the large TPA cross sections compared to those of the complexes **5**, **6**, **8** and ligands (L^1, L^2).

Conclusions

In summary, eight novel Ag(ɪ) coordination polymers or discrete supramolecular complexes (**1**–**8**) with rigid multidentate ligands (L^1 and L^2) have been prepared and structurally characterized. Single crystal X-ray structures indicated that the ligands adopted several coordination modes to coordinate with Ag(ɪ) ions in the complexes. The complexes exhibit different molecular structures and packing characteristics suggesting that the ligands, the solvents and the counteranions have a subtle but important influence on the structure of the complexes. In addition, the third-order NLO properties of the complexes were investigated in detail, and the results showed that complexes **1**, **2**, **3**, **4** and **7** may be good candidates for non-linear optical materials.

Acknowledgements

Notes and references

1 (a) C. Q. Wan and T. C. W. Mak, *Cryst. Growth Des.*, 2011, **11**, 832; (b) L. Han, H. Valle and X. H. Bu, *Inorg. Chem.*, 2007, **46**, 1511; (c) E. Y. Cheung, K. Fujii, F. Guo, K. D. M. Harris, S. Hasebe and R. Kuroda, *Cryst. Growth Des.*, 2011, **11**, 3313; (d) D. Singh and J. B. Baruah, *Cryst. Growth Des.*, 2011, **11**, 768; (e) H. K. Liu, W. Y. Sun and W. X. Tang, *J. Chem. Soc., Dalton Trans.*, 2002, 3886; (f) E. Yang, J. Zhang and Y. G. Yao, *Inorg. Chem.*, 2004, **43**, 6525.

2 (a) G. A. Farnum, C. M. Gandolfo, R. M. Supkowski and R. L. LaDuca, *Cryst. Growth Des.*, 2011, **11**, 4860; (b) D. M. Shin, I. S. Lee, Y. A. Lee and Y. K. Chung, *Inorg. Chem.*, 2003, **42**, 2977; (c) T. Honda, T. Nakanishi and K. Ohkubo, *J. Am. Chem. Soc.*, 2010, **132**, 10155; (d) R. Nuria, B. Adrien, L. B. Patrice, L. B. Hubert, A. Chantal, B. Sophie, C. Christophe and M. Olivier, *Chem. Mater.*, 2011, **23**, 3228.

3 (a) S. Natarajan and P. Mahata, *Curr. Opin. Solid State Mater. Sci.*, 2009, **13**, 46; (b) J. P. Zhang, Y. B. Zhang, J. B. Lin and X. M. Chen, *Chem. Rev.*, 2012, **112**, 1001.

4 (a) H. W. Hou, Y. L. Wei, Y. L. Song, L. M. Mi, M. S. Tang, L. K. Li and Y. T. Fan, *Angew. Chem., Int. Ed.*, 2005, **44**, 6067; (b) C. Zhang, Y. L. Song and X. Wang, *Coord. Chem. Rev.*, 2007, **251**, 111; (c) Z. Xu, K. H. Baek, H. N. Kim, J. Cui, X. Qian, D. R. Spring, I. Shin and J. Yoon, *J. Am. Chem. Soc.*, 2010, **132**, 601; (d) M. K. Kim, C. S. Lim, J. T. Hong, J. H. Han, H. Y. Jang, H. M. Kim and B. R. Cho, *Angew. Chem., Int. Ed.*, 2010, **49**, 364.

5 (a) Y. Yu, J. P. Ma and Y. B. Dong, *CrystEngComm*, 2012, **14**, 7157; (b) Z. G. Gu, Y. T. Liu, X. J. Hong, Q. G. Zhan, Z. P. Zheng, S. R. Zheng, W. S. Li, S. J. Hu and Y. P. Cai, *Cryst. Growth Des.*, 2012, **12**, 2178; (c) G. G. Hou, Y. Wu, J. P. Ma and Y. B. Dong, *CrystEngComm*, 2011, **13**, 6850; (d) Z. G. Gu, H. C. Fang, P. Y. Yin, L. Tong, Y. B. Ying, S. J. Hu, W. S. Li and Y. P. Cai, *Cryst. Growth Des.*, 2011, **11**, 2220; (e) M. A. Haj, C. B. Aakeröy and J. Desper, *New J. Chem.*, 2013, **37**, 204.

6 Z. Zheng, Z. P. Yu, M. D. Yang, F. Jin, Q. Zhang, H. P. Zhou, J. Y. Wu and Y. P. Tian, *J. Org. Chem.*, 2013, **78**, 3222.

7 (a) G. Mukherjee, P. Singh, C. Ganguri, S. Sharma, H. B. Singh, N. Goel, U. P. Singh and R. J. Butcher, *Inorg. Chem.*, 2012, **51**, 8128; (b) P. J. Yang, F. J. Cui, X. J. Yang and B. Wu, *Cryst. Growth Des.*, 2013, **13**, 186; (c) B. Li, S. Q. Zang, C. Ji, H. W. Hou and T. C. W. Mak, *Cryst. Growth Des.*, 2012, **12**, 1443; (d) P. C. Cheng, C. W. Yeh, W. Hsu, T. R. Chen, H. W. Wang, J. D. Chen and J. C. Wang, *Cryst. Growth Des.*, 2012, **12**, 943; (e) S. Park, L. F. Lindoy and S. S. Lee, *Cryst. Growth Des.*, 2012, **12**, 1320.

8 (a) L. Poorters, D. Armspach, D. Matt, L. Toupet and P. G. Jones, *Angew. Chem., Int. Ed.*, 2007, **46**, 2663; (b) O. S. Jung, Y. A. Lee, Y. J. Kim and J. K. Hong, *Cryst. Growth Des.*, 2002, **2**, 497; (c) M. R. Sambrook, P. D. Beer, J. A. Wisner, R. L. Paul, A. R. Cowley, F. Szemes and M. G. B. Drew, *J. Am. Chem. Soc.*, 2005, **127**, 2292; (d) C. S. Campos-Fernández, B. L. Schottel, H. T. Chifotides, J. K. Bera, J. Bacsa, J. M. Koomen, D. H. Russell and K. R. Dunbar, *J. Am. Chem. Soc.*, 2005, **127**, 12909.

9 (a) I. D. Giles, H. T. Chifotides, M. Shatruk and K. R. Dunbar, *Chem. Commun.*, 2011, **47**, 12604; (b) C. S. Campos-Fernandez, B. L. Schottel, H. T. Chifotides, J. K. Bera, J. Bacsa, J. M. Koomen, D. H. Russell and K. R. Dunbar, *J. Am. Chem. Soc.*, 2005, **127**, 12909; (c) S. R. Halper, L. Do, J. R. Stork and S. M. Cohen, *J. Am. Chem. Soc.*, 2006, **128**, 15255; (d) L. S. Song, H. M. Wang, Y. Y. Niu, H. W. Hou and Y. Zhu, *CrystEngComm*, 2012, **14**, 4927; (e) I. Bassanetti,

F. Mezzadri, A. Comotti, P. Sozzani, M. Gennari, G. Calestani and L. Marchiò, *J. Am. Chem. Soc.*, 2012, **134**, 9142.

10 J. L. Gulbransen and C. M. Fitchett, *CrystEngComm*, 2012, **14**, 5394.

11 (a) Y. Zuo, M. Fang, G. Xiong, P. F. Shi, B. Zhao, J. Z. Cui and P. Cheng, *Cryst. Growth Des.*, 2012, **12**, 3917; (b) H. P. Zhou, P. Wang, Z. J. Hu, L. Li, J. J. Chen, Y. Cui, Y. P. Tian, J. Y. Wu, J. X. Yang, X. T. Tao and M. H. Jiang, *Eur. J. Inorg. Chem.*, 2007, 1854; (c) H. P. Zhou, Y. P. Tian, J. Y. Wu, J. Z. Zhang, D. M. Li, Y. M. Zhu, Z. J. Hu, X. T. Tao, M. H. Jiang and Y. Xie, *Eur. J. Inorg. Chem.*, 2005, 4976; (d) F. Jin, X. F. Yang, S. L. Li, Z. Zheng, Z. P. Yu, L. Kong, F. Y. Hao, J. X. Yang, J. Y. Wu, Y. P. Tian and H. P. Zhou, *CrystEngComm*, 2012, **14**, 8409.

12 J. Guo, C. P. Li and M. Du, *Inorg. Chim. Acta*, 2013, **395**, 212.

13 J. L. Gulbransen and C. M. Fitchett, *CrystEngComm*, 2012, **14**, 5394.

14 (a) F. Luo, S. R. Batten, Y. Che and J. M. Zheng, *Chem.–Eur. J.*, 2007, **13**, 4948; (b) Z. S. Bai, J. Xu, T. A. Okamura, M. S. Chen, W. Y. Sun and N. Ueyama, *Dalton Trans.*, 2009, 2528.

15 K. Chainok, S. M. Neville, C. M. Forsyth, W. J. Gee, K. S. Murray and S. R. Batten, *CrystEngComm*, 2012, **14**, 3717.

16 D. M. Li, Q. Z. Wang, P. J. Y. Wu, Y. H. Kan, Y. P. Tian, H. P. Zhou, J. X. Yang, X. T. Tao and M. H. Jiang, *Dalton Trans.*, 2011, **40**, 8170.

17 T. Geethakrishnan and P. K. Palanisamy, *Opt. Commun.*, 2007, **270**, 424.

18 (a) J. F. Ge, Y. T. Lu, R. Sun, J. Zhang, Q. F. Xu, N. J. Li, Y. L. Song and J. M. Lu, *Dyes Pigm.*, 2011, **91**, 489; (b) J. Mattu, T. G. Johansson and W. Leach, *J. Phys. Chem. C*, 2007, **111**, 6868.

19 (a) T. Xia, D. J. Hagan, M. Sheik-Bahae and E. W. Van Stryland, *Opt. Lett.*, 1994, **19**, 317; (b) I. L. Bolotin, D. J. Asunskis, A. M. Jawaid, Y. M. Liu, P. T. Snee and L. Hanley, *J. Phys. Chem. C*, 2010, **114**, 16257.

20 (a) E. Collini, *Phys. Chem. Chem. Phys.*, 2012, **14**, 3725; (b) F. C. Spano and S. Mukamel, *J. Chem. Phys.*, 1991, **95**, 7526; (c) F. C. Spano, *Phys. Rev. Lett.*, 1991, **67**, 3424; (d) F. C. Spano, *Phys. Rev. Lett.*, 1992, **68**, 2976.

21 (a) S. Das, A. Nag, D. Goswami and P. K. Bharadwaj, *J. Am. Chem. Soc.*, 2006, **128**, 402; (b) F. X. Zhou, Z. Zheng, H. P. Zhou, W. Z. Ke, J. Q. Wang, Z. P. Yu, F. Jin, J. X. Yang, J. Y. Wu and Y. P. Tian, *CrystEngComm*, 2012, **14**, 5613.